

# Nature of chiral phase transition of two flavour QCD from imaginary chemical potential with HISQ fermions

Liang-Kai Wu\*

*Faculty of Science, Jiangsu University, Zhenjiang 212013, People's Republic of China  
National Supercomputer Center in Wuxi, Wuxi, Jiangsu, 214072, People's Republic of China and  
Department of Physics, College of Science, Swansea University, Swansea, SA2 8PP, UK*

Fa-Ling Zhang

*Faculty of Science, Jiangsu University, Zhenjiang 212013, People's Republic of China*

(Dated: December 3, 2024)

The nature of thermal phase transition of two flavour Quantum Chromodynamic (QCD) in the chiral limit has important implication for the QCD phase diagram. We carry out lattice QCD simulations to address this problem. Results on the nature of phase transition of  $N_f = 2$  QCD in the chiral limit are presented. Simulations are conducted with a Symanzik-improved gauge action and the HISQ fermion action. Within the imaginary chemical potential formulation, five different quark masses  $am = 0.020, 0.018, 0.015, 0.013, 0.010$ , and four different lattice volumes,  $N_s = 8, 12, 16, 20$ , are used to explore the scaling behaviour. By interpreting the intersection point of the Binder cumulant of the chiral condensate on different lattice volumes as the critical phase transition point, we obtain the critical imaginary chemical potential values at each of five quark masses. A positive value  $(\mu/T)_{tric}^2 = 0.172(16)$  is obtained after extrapolation of the  $Z(2)$  transition line to the chiral limit by taking advantage of the known critical exponents at the tricritical point. Result on our coarse lattice  $N_t = 4$  suggests that the nature of the phase transition of two flavour QCD in the chiral limit is of first order.

PACS numbers: 12.38.Gc, 11.10.Wx, 11.15.Ha, 12.38.Mh

## I. INTRODUCTION

The thermodynamics of matter described by QCD is characterized by a transition from the low-temperature hadronic phase with confined quarks and gluons to the high-temperature phase with deconfined quarks and gluons. The phase transition of this matter is relevant to the early Universe, compact stars and heavy ion collision experiments. Reviews on the study of the phase diagram can be found in Refs. [1–3] and references therein. Mapping out the phase diagram of QCD is one of the most challenging tasks presented for theoretical physics. Although substantial progress has been achieved in determining the phase diagram of QCD at zero density, the nature of the phase transition of QCD with two massless flavours remains still open.

At the transition point, if the  $U_A(1)$  symmetry is not restored, QCD with two massless flavours has the symmetry-breaking pattern  $[SU(2)_L \times SU(2)_R]/Z(2)_V \rightarrow SU(2)_V/Z(2)_V$ , on the other hand, if the  $U_A(1)$  symmetry is effectively and fully restored, QCD with two massless flavours has the symmetry-breaking pattern  $[U(2)_L \times U(2)_R]/U(1)_V \rightarrow U(2)_V/U(1)_V$  [4–6]. For two flavour QCD, Pisarsky and Wilczek pointed out that if the  $U_A(1)$  symmetry is broken at transition point  $T_c$ , the system undergoes second order transition with  $O(4)$  scaling, although not necessarily. On the other hand, if the

$U_A(1)$  symmetry is restored at  $T_c$ , the system undergoes a first order transition. However, further studies [5, 6] show that even if the  $U_A(1)$  symmetry is restored at  $T_c$ , the system also may have an infrared fixed point, so the transition can be of either first order or second order with different critical exponents from the  $O(4)$  universality class. Ref. [7] suggests the transition is of second order, but yet one of critical exponents is different from the standard  $O(4)$  model.

As the interaction between the quarks and gluons is inherently strong on hadronic energy scales, lattice QCD simulation is the most reliable method up to date. The standard method to address the nature of QCD with two massless flavours is to carry out simulations by successively reducing the quark mass, and in the meantime, monitoring the transition behaviour. If the transition is of second order in the chiral limit, then this second transition disappears immediately when finite quark masses are turned on. On the other hand, if the transition is of first order in the chiral limit, it will get weakened gradually until at a certain  $Z(2)$  point as the finite quark masses increase.

Considerable work using lattice QCD simulations has been devoted to this problem. Some lattice QCD simulation studies favour a second order transition [8–15], some support that the transition is of first order [16–21] and some favour neither [22, 23]. For a discussion, see Refs. [12, 16, 24] and references therein.

Apart from the conventional method which focuses on the critical exponents, the nature of the phase transition of QCD with two massless flavours can be addressed by

---

\*Corresponding author. Email address: wuliangkai@163.com

exploring the fate of  $U_A(1)$  symmetry at high temperature [20, 21, 25]. Ref. [18] discusses this problem from the aspect of non-integer numbers of flavors. In Ref. [16], a novel approach has been developed to address the nature the phase transition of QCD with two massless flavours within the staggered fermion formulation, and this approach is employed in Ref. [17] within the Wilson fermion formulation. The approach takes advantage of the fact that when the imaginary chemical potential is switched on, the second order line which separates the first order region from the crossover region is governed by the tricritical scaling law, and the critical exponents around  $am = 0$  are known [16, 17, 26].

So far, the investigation to address the nature of the phase transition of QCD with two massless flavours using this method are implemented through standard gauge and fermion actions [16, 17]. Standard KS fermions suffer from taste symmetry breaking at nonzero lattice spacing  $a$  [27]. This taste symmetry breaking can be illustrated by the smallest pion mass taste splitting which is comparable to the pion mass even at lattice spacing  $a \sim 0.1fm$  [28].

In this paper, we aim to investigate the nature of the phase transition of QCD with two massless flavours with a one-quark-loop Symanzik-improved gauge action [29–34] and the HISQ action [35]. The one-quark-loop Symanzik-improved gauge action has discretization error of  $O(\alpha_s^2 a^2, a^4)$ , and the HISQ action completely eliminates the  $O(a^2)$  error at tree level by including smeared one-link and "Naik terms" [36, 37]. Moreover, the HISQ action yields the smallest violation of taste symmetry among the currently used staggered actions [27, 38, 39]. These improvements are significant on the  $N_t = 4$  lattice where the lattice spacing is quite large.

The paper is organized as follows: In Sec. II, we define the lattice action with imaginary chemical potential and the physical observables we calculate. Our simulation results are presented in Sec. III, followed by discussion in Sec. IV.

## II. LATTICE FORMULATION WITH IMAGINARY CHEMICAL POTENTIAL

After introducing a pseudofermion field  $\Phi$ , the partition function of the system can be represented as:

$$Z = \int [dU][d\Phi^*][d\Phi] e^{-S_g - S_f},$$

where  $S_g$  is the Symanzik-improved gauge action, and  $S_f$  is the HISQ quark action with the quark chemical potential  $\mu$ . Here  $\mu = i\mu_I$  is purely imaginary. For  $S_g$ , we use

$$S_g = \beta \left( C_P \sum_{x;\mu<\nu} (1 - P_{\mu\nu}) + C_R \sum_{x;\mu\neq\nu} (1 - R_{\mu\nu}) + C_T \sum_{x;\mu<\nu<\sigma} (1 - T_{\mu\nu\sigma}) \right),$$

with  $P_{\mu\nu}$ ,  $R_{\mu\nu}$  and  $T_{\mu\nu\sigma}$  standing for 1/3 of the real part of the trace of  $1 \times 1$ ,  $1 \times 2$  planar Wilson loops and  $1 \times 1 \times 1$  "parallelogram" loops, respectively.

$$P_{\mu\nu} = \frac{1}{3} \text{ReTr} \left[ \begin{array}{c} \leftarrow \\ \square \\ \rightarrow \end{array} \right],$$

$$R_{\mu\nu} = \frac{1}{3} \text{ReTr} \left[ \begin{array}{c} \leftarrow \quad \leftarrow \\ \square \\ \rightarrow \quad \rightarrow \end{array} \right],$$

$$T_{\mu\nu\sigma} = \frac{1}{3} \text{ReTr} \left[ \begin{array}{c} \leftarrow \quad \leftarrow \\ \diagup \quad \diagdown \\ \rightarrow \quad \rightarrow \end{array} \right].$$

The coefficients  $C_P, C_R, C_T$  are tadpole improved [39],

$$\begin{aligned} C_P &= 1.0, \\ C_R &= \frac{-1}{20u_0^2} (1 - (0.6264 - 1.1746n_f) \ln(u_0)), \\ C_T &= \frac{1}{u_0^2} (0.0433 - 0.0156n_f) \ln(u_0). \end{aligned}$$

with  $u_0 = (\langle P_{\mu\nu} \rangle)^{3/4}$ .

The HISQ action with pseudofermion field  $\Phi$  is

$$S_f = \left\langle \Phi \left| [M^\dagger[U]M[U]]^{-n_f/4} \right| \Phi \right\rangle,$$

where the form of  $M_{x,y}[U] = 2m_{x,y} + 2\mathcal{D}_{x,y}(U)$  reading

$$\begin{aligned} 2\mathcal{D}_{x,y} &= \sum_{\rho=1}^3 \{ X_\rho(x) \delta_{x+\hat{\rho},y} - X_\rho^\dagger(x-\hat{\rho}) \delta_{x-\hat{\rho},y} \} \\ &+ \sum_{\rho=1}^3 \{ N_\rho(x) \delta_{x+3\hat{\rho},y} - N_\rho^\dagger(x-3\hat{\rho}) \delta_{x-3\hat{\rho},y} \} \\ &+ \left\{ e^{ia\mu_I} X_4(x) \delta_{x+\hat{4},y} - e^{-ia\mu_I} X_4^\dagger(x-\hat{4}) \delta_{x-\hat{4},y} \right\} \\ &+ \left\{ e^{i3a\mu_I} N_4(x) \delta_{x+3\hat{4},y} - e^{-i3a\mu_I} N_4^\dagger(x-3\hat{4}) \delta_{x-3\hat{4},y} \right\} \end{aligned} \quad (1)$$

The Dirac operator  $\mathcal{D}$  is constructed from smeared links [39]. The fundamental gauge links are  $U_\mu(x)$ , the fat links after a level one fat7 smearing are  $V_\mu(x)$ , the reunitarized links are  $W_\mu(x)$ , and the fat links after level two asqtad smearing are  $X_\mu(x)$ . For simplicity, we use  $N_{x,\rho} = W_\rho(x)W_\rho(x+\hat{\rho})W_\rho(x+2\hat{\rho})$ . The staggered

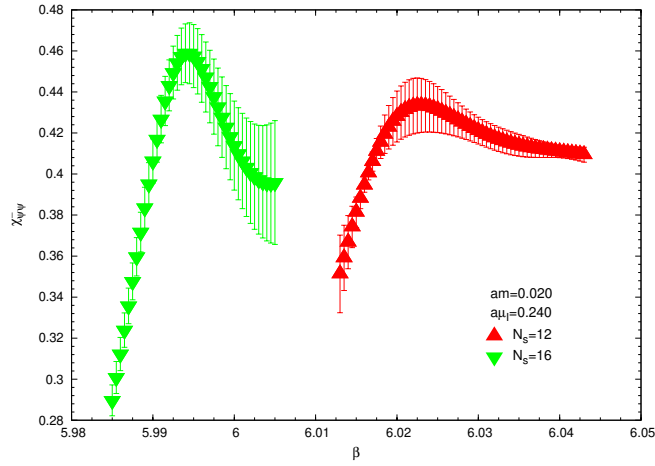


FIG. 1: Susceptibility of chiral condensate  $\chi_{\bar{\psi}\psi}$  as a function of coupling  $\beta$  at quark mass  $am = 0.020$  on lattice  $12^3 \times 4$  and  $16^3 \times 4$ .

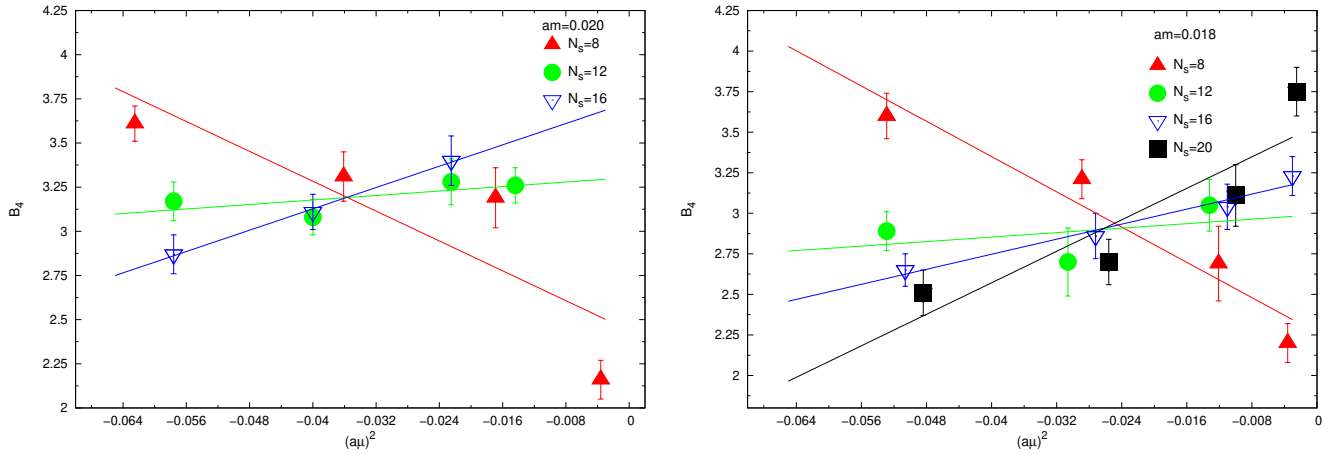


FIG. 2: Binder cumulants of  $\bar{\psi}\psi$  at quark mass  $am = 0.020$  (left panel) and  $am = 0.018$  (right panel) on different lattice volumes intersect at one point.

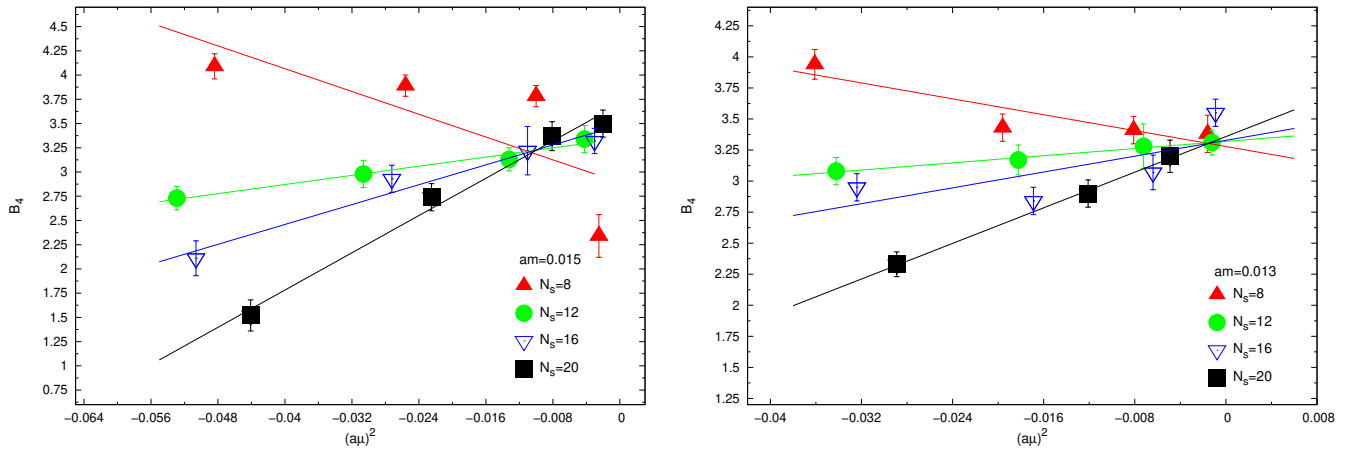


FIG. 3: Binder cumulants of  $\bar{\psi}\psi$  at quark mass  $am = 0.015$  (left panel) and  $am = 0.013$  (right panel) on different lattice volumes intersect at one point.

fermion phases are absorbed into the link variables.  $\hat{\rho}$ ,  $\hat{4}$  are the unit vector along  $\rho$ -direction, 4-direction, re-

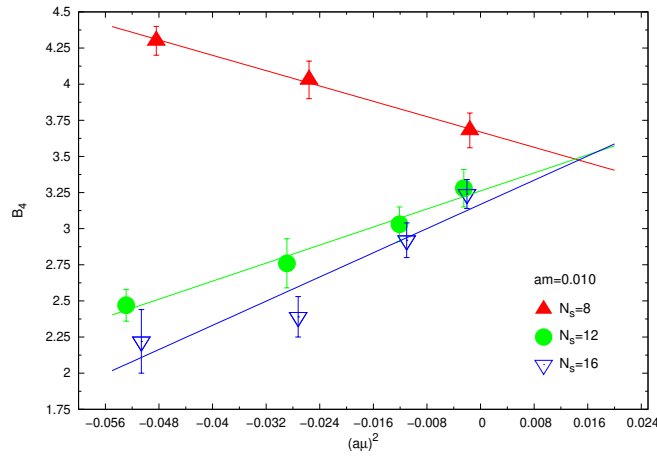


FIG. 4: Binder cumulants of  $\bar{\psi}\psi$  at quark mass  $am = 0.010$  on different lattice volumes intersect at one point.

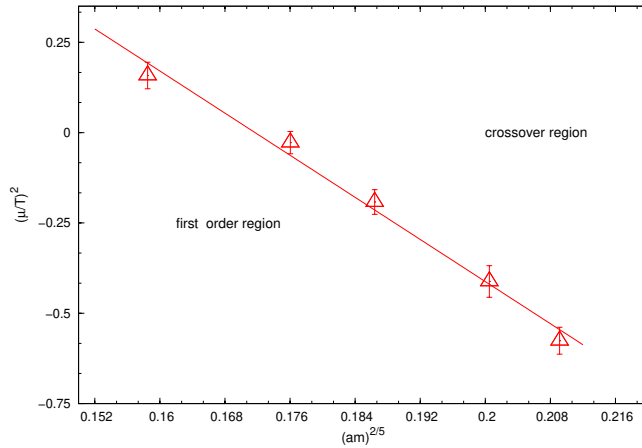


FIG. 5:  $Z(2)$  critical points at different quark masses form a curve which extrapolated to the zero quark mass limit by using the tricritical exponents.

spectively.

In the study to address the chiral transition, it is natural to choose the chiral condensate as our observable. The chiral condensate is defined as:

$$X = \bar{\psi}\psi = \frac{1}{N_s^3 N_t} \text{Tr}(M^{-1}),$$

$N_s, N_t$  are the spatial, and temporal extent of lattice, respectively. To simplify notation, we use  $X$  to represent the chiral condensate. The susceptibility of chiral condensate is defined as

$$\chi_{\bar{\psi}\psi} = \langle (X - \langle X \rangle)^2 \rangle.$$

We also calculate the Binder cumulant of chiral condensate which is defined as:

$$B_4 = \langle (X - \langle X \rangle)^4 \rangle / \langle (X - \langle X \rangle)^2 \rangle^2. \quad (2)$$

The Binder cumulant of chiral condensate can be expanded around  $a\mu_c$  as [16, 17]

$$B_4(m, a\mu) = B_4(m, a\mu_c) + b_1((a\mu)^2 - (a\mu_c)^2)N_s^{1/\nu} + \dots \quad (3)$$

To be self-contained, we summarize the strategy to determine the nature of the phase transition of QCD with two massless flavours which is presented in Ref. [16].

1. At a certain quark mass  $am$ , we first determine the  $Z_2$  transition point by scanning the imaginary chemical potential on different lattice volumes. This can be achieved by interpreting the intersection point of Binder cumulant on different lattice volumes as the critical transition point.
2. Those  $Z_2$  transition points form a curve.
3. Extrapolate the  $Z_2$  transition line to the chiral limit to get  $(\mu/T)_{tric}^2$  by assuming the line is governed by the power law

$$(am_q)^{2/5} = C [(\mu/T)^2 - (\mu/T)_{tric}^2]. \quad (4)$$

In the  $(\mu/T)^2 - am$  plane, we assume the  $Z_2$  transition line connects the two tricritical points. One of

the two tricritical points is at the  $(\mu/T)^2$  axis, the other is at the  $am$  axis. When we extend the  $Z_2$  transition line to massless limit, the  $Z_2$  transition line will intersect with the  $(\mu/T)^2$  axis at the tricritical point at the  $(\mu/T)^2_{tric}$  axis.  $(\mu/T)^2_{tric}$  is the value at such a intersection point at the  $(\mu/T)^2$  axis. This scenario is illustrated in Fig. 7 in Ref. [16] and Fig. 2 in Ref. [17].

4. Check the value of  $(\mu/T)^2_{tric}$  to see whether it is bigger (corresponding to first order) or smaller than ( corresponding to second order) 0.

### III. MC SIMULATION RESULTS

Before presenting the simulation results, we describe the computation details. Simulations are carried out at quark mass  $am = 0.020, 0.018, 0.015, 0.013, 0.010$ . Rational Monte Carlo algorithm [40–42] is used to generate configurations. We used different molecular dynamics step sizes for the gauge and fermion parts of the action, with three gauge steps for each fermion step [43]. The Omelyan integration algorithm [44, 45] is employed for the gauge and fermion action. For the molecular dynamics evolution, we use a 9'th rational function to approximate  $[M^+(U)M(U)]^{-n_f/4}$  for the pseudofermion field. For the heat bath updating and for computing the action at the beginning and end of the molecular dynamics trajectory, 10'th rational function is used to approximate  $[M^+(U)M(U)]^{n_f/8}$  and  $[M^+(U)M(U)]^{-n_f/8}$ , respectively. The step is chosen to ensure the acceptance rate is around 72%–82%. 5,000 trajectories of configuration are taken as warmup from a cold start. In order to fill in observables at additional  $\beta$  values, we employ the Ferrenberg-Swendsen reweighting method [46].

At a certain quark mass  $am$  and  $a\mu_I$ , we scan the  $\beta$  values to calculate the susceptibility  $\chi_{\bar{\psi}\psi}$  of chiral condensate  $\bar{\psi}\psi$ . The location of peak of susceptibility of chiral condensate is interpreted as the transition point. For clarity, we only present the results of  $\chi_{\bar{\psi}\psi}$  on lattice  $N_s = 12$  and  $N_s = 16$  at  $am = 0.020$  in Fig 1. Similar behaviour of  $\chi_{\bar{\psi}\psi}$  can be observed at other couples of  $(am, a\mu_I)$  values on different lattice volumes.

The results of critical couplings  $\beta_c$ , and the corresponding  $B_4$  values on different spatial volumes at different quark masses  $am$  are summarized in Table. I. These  $\beta_c$ 's are determined from the locations of peak susceptibility  $\chi_{\bar{\psi}\psi}$  of chiral condensate  $\bar{\psi}\psi$ .

After the critical couplings  $\beta_c$ , and the corresponding  $B_4$  values are obtained, we can monitor their behaviour on different lattice spatial volume at one quark mass. The results are presented in Fig. 2,3,4. From Fig. 2,3,4, we can find that with decreasing absolute value of chemical potential, the  $B_4$  value increases on lattice  $N_s = 12, 16$  and  $N_s = 20$ , on the contrary, on lattice  $N_s = 8$ , the values of  $B_4$  fall with declining absolute value of chemical potential. However, at a certain quark mass, we can find

that the  $B_4$  values on different lattice volume intersect approximately at one point which is interpreted as the critical  $Z(2)$  transition point. By fitting the  $B_4$  values to Eq. 3, the critical  $a\mu_c$  can be achieved. The results are presented in Table II.

After the  $Z(2)$  transition points at five quark masses are obtained, we plot the change of  $a\mu_c$ 's with quark masses  $am$  in Fig. 5. The quark mass axis and chemical potential axis are rescaled with the appropriate critical exponents to make the linear relationship clearer. From Fig. 5, we can find that the data points follow a linear relationship, despite the quark masses are relatively large. We use the Eq. 4 to extrapolate the  $Z(2)$  transition line to the chiral limit to estimate  $(\mu/T)^2_{tric}$  at the tricritical point. The result is  $(\mu/T)^2_{tric} = 0.172(16)$  with  $\chi^2 = 0.36$ .

### IV. DISCUSSIONS

We have studied the nature of the phase transition of QCD with two massless flavours with a one-quark-loop Symanzik-improved gauge action and the HISQ fermion action by using the method proposed in Ref. [16]. In the imaginary chemical potential region, our simulation shows that with the decrease of absolute value of imaginary chemical potential, the first order region extends from the imaginary chemical potential region to the real chemical potential region.

The  $Z(2)$  transition line which governed by the tricritical power law is extrapolated to the chiral limit. The positive value of  $(\mu/T)^2_{tric} = 0.172(16)$  at zero quark mass implies the phase transition of QCD with two massless flavours is of first order on  $N_t = 4$ , coarse lattice.

In our simulation at quark mass  $am = 0.010$ , the Binder cumulant values  $B_4$  of chiral condensate on three lattice volumes intersect at a positive squared chemical potential value. This implies that the  $Z(2)$  transition line extends to the real chemical potential region. This result also shows that the phase transition of two massless QCD is of first order.

In our simulation, we find that the Binder cumulants of chiral condensate on different lattice volumes at one quark mass intersect at one point. The value of  $B_4$  at the intersection point is renormalization-invariant. Its value should be 1.604 [16, 17]. However, in our simulation, The value of  $B_4$  at the intersection point is around 3.

From Eq. 3, we expect that the behaviour of Binder cumulant of chiral condensate  $B_4$  on different lattice volume have the same tendency of change. However, the change trend of  $B_4$  with chemical potential on the lattice  $N_s = 8$  is on the opposing trend of those on lattice  $N_s = 12, 16, 20$ .

In our simulation, from Fig. 2,3,4, we can find that the interval between  $a\mu_I$  values which we use in our simulation is large. Some  $a\mu_I$  values are far from the intersection point. This situation makes the intersection point sensitive to  $B_4$  values.

TABLE I: Results of critical couplings  $\beta_c$  obtained by interpreting the locations of peak of  $\chi_{\bar{\psi}\psi}$ , and the  $B_4$  values on different spatial volume at different quark masses  $am$ .

am	$N_s = 8$			$N_s = 12$			$N_s = 16$			$N_s = 20$		
	$a\mu_I$	$\beta_c$	$B_4$	$a\mu_I$	$\beta_c$	$B_4$	$a\mu_I$	$\beta_c$	$B_4$	$a\mu_I$	$\beta_c$	$B_4$
0.010	0.040	5.998(40)	3.68(12)	0.050	6.058(20)	3.28(13)	0.045	6.018(20)	3.25(10)	-	-	-
	0.100	6.018(40)	5.33(12)	0.110	6.048(20)	3.04(12)	0.105	5.998(20)	2.93(12)	-	-	-
	0.160	6.008(20)	4.03(13)	0.170	5.988(60)	2.77(17)	0.165	5.998(40)	2.39(14)	-	-	-
0.013	0.220	5.988(20)	4.31(10)	0.230	6.048(20)	2.48(11)	0.225	6.098(20)	2.22(22)	-	-	-
	0.040	5.998(40)	3.39(15)	0.035	6.008(60)	3.31(10)	0.030	6.008(60)	3.55(11)	-	-	-
	0.090	5.998(20)	3.42(11)	0.085	5.968(40)	3.28(18)	0.080	6.008(10)	3.08(14)	0.070	6.048(10)	3.21(13)
0.015	0.140	5.988(30)	3.43(11)	0.135	5.988(28)	3.17(12)	0.130	5.964(30)	2.23(11)	0.110	6.048(30)	2.91(11)
	0.190	6.048(24)	3.94(12)	0.185	5.984(34)	3.09(11)	0.180	6.090(30)	1.84(11)	0.170	6.098(50)	2.34(10)
	0.050	6.078(30)	2.35(22)	0.065	6.018(20)	3.35(14)	0.055	5.988(30)	3.33(13)	0.045	6.028(20)	3.51(14)
0.018	0.100	5.968(40)	3.78(11)	0.115	6.008(70)	3.14(12)	0.105	5.988(20)	3.22(25)	0.090	6.028(20)	3.37(15)
	0.160	6.028(30)	3.90(11)	0.175	6.068(110)	2.98(14)	0.165	6.058(30)	2.93(14)	0.150	6.098(10)	2.74(14)
	0.220	5.988(10)	4.10(13)	0.230	6.028(20)	2.74(12)	0.225	5.968(100)	2.12(18)	0.210	5.968(10)	1.52(16)
0.020	0.060	5.978(30)	2.20(12)	0.065	6.018(20)	3.05(10)	0.055	6.018(40)	3.24(12)	0.050	6.058(10)	3.75(15)
	0.110	5.958(50)	2.69(23)	0.115	5.978(50)	3.05(16)	0.105	6.018(10)	3.04(14)	0.100	5.978(40)	3.12(19)
	0.170	5.968(90)	3.22(12)	0.175	5.968(40)	2.70(21)	0.165	5.998(30)	2.86(14)	0.160	5.978(10)	2.70(14)
0.020	0.230	5.988(30)	3.61(14)	0.235	6.028(20)	2.89(12)	0.225	6.018(20)	2.65(10)	0.220	5.988(40)	2.51(14)
	0.060	5.998(20)	2.16(11)	0.120	6.005(30)	3.26(10)	0.120	6.038(80)	3.10(16)	-	-	-
	0.130	5.998(90)	3.19(17)	0.150	6.078(70)	3.28(13)	0.150	6.018(40)	3.40(14)	-	-	-
0.020	0.190	6.048(40)	3.31(14)	0.240	6.058(30)	3.08(10)	0.200	6.078(40)	3.12(10)	-	-	-
	0.250	5.998(20)	3.62(10)	0.240	6.025(10)	3.18(10)	0.240	5.998(50)	2.87(11)	-	-	-

TABLE II: Results of critical chemical potential  $a\mu_c$  at different quark masses obtained by fitting Eq. (3) to data on different spatial volumes. Value of critical chemical potential  $a\mu_c$  at  $am = 0.010$  is real, while values of critical chemical potential  $a\mu_c$  at other quark masses are purely imaginary.

$am$	$a\mu_c$	$r$ -square
0.010	0.099(37)	0.62
0.013	0.042(31)	0.92
0.015	0.109(34)	0.77
0.018	0.160(44)	0.89
0.020	0.189(37)	0.27

Ref. [47] employs the HISQ fermions to investigate the

critical endpoint of three flavour QCD at zero density, the result favours a small first order region. Also, simulation in Ref. [48–50] show that the first order region shrinks on finer lattice, this situation calls for the simulation towards the continuum limit.

#### Acknowledgments

We thank Gert Aarts, Simon Hands, Chris Allton for valuable help. We modified the MILC collaboration's public code [51] to simulate the theory at imaginary chemical potential. We used the fortran-90 based multi-precision software [52]. This work is supported by the National Science Foundation of China (NSFC) under Grant Nos. (11347029) and the National Fund for Studying Abroad of China. The work was carried out at the National Supercomputer Center in Wuxi and the National Supercomputer Center in Tianjin.

[1] K. Fukushima and T. Hatsuda, Rept. Prog. Phys. **74** 014001 (2011).  
[2] K. Fukushima, J. Phys. G **39** 013101 (2012).  
[3] G. Aarts, J. Phys. Conf. Ser. **706**, no. 2, 022004 (2016) doi:10.1088/1742-6596/706/2/022004 [arXiv:1512.05145 [hep-lat]].

[4] R. D. Pisarski and F. Wilczek, Phys. Rev. D **29**, 338 (1984). doi:10.1103/PhysRevD.29.338  
[5] A. Butti, A. Pelissetto and E. Vicari, JHEP **0308**, 029 (2003) doi:10.1088/1126-6708/2003/08/029 [hep-ph/0307036].  
[6] A. Pelissetto and E. Vicari, Phys. Rev. D **88**,

- no. 10, 105018 (2013) doi:10.1103/PhysRevD.88.105018 [arXiv:1309.5446 [hep-lat]].
- [7] T. Sato and N. Yamada, Phys. Rev. D **91**, no. 3, 034025 (2015) doi:10.1103/PhysRevD.91.034025 [arXiv:1412.8026 [hep-lat]].
- [8] S. Ejiri *et al.*, Phys. Rev. D **80**, 094505 (2009) doi:10.1103/PhysRevD.80.094505 [arXiv:0909.5122 [hep-lat]].
- [9] F. Karsch and E. Laermann, Phys. Rev. D **50**, 6954 (1994) doi:10.1103/PhysRevD.50.6954 [hep-lat/9406008].
- [10] A. Ali Khan *et al.* [CP-PACS Collaboration], Phys. Rev. D **63**, 034502 (2001) doi:10.1103/PhysRevD.63.034502 [hep-lat/0008011].
- [11] S. Ejiri, R. Iwami and N. Yamada, Phys. Rev. D **93**, no. 5, 054506 (2016) doi:10.1103/PhysRevD.93.054506 [arXiv:1511.06126 [hep-lat]].
- [12] F. Burger *et al.* [tmfT Collaboration], Phys. Rev. D **87**, no. 7, 074508 (2013) doi:10.1103/PhysRevD.87.074508 [arXiv:1102.4530 [hep-lat]].
- [13] S. Aoki *et al.* [JLQCD Collaboration], Phys. Rev. D **57**, 3910 (1998) doi:10.1103/PhysRevD.57.3910 [hep-lat/9710048].
- [14] C. W. Bernard *et al.*, Phys. Rev. Lett. **78**, 598 (1997) doi:10.1103/PhysRevLett.78.598 [hep-lat/9611031].
- [15] Y. Iwasaki, K. Kanaya, S. Kaya and T. Yoshie, Phys. Rev. Lett. **78**, 179 (1997) doi:10.1103/PhysRevLett.78.179 [hep-lat/9609022].
- [16] C. Bonati, P. de Forcrand, M. D'Elia, O. Philipsen and F. Sanfilippo, Phys. Rev. D **90**, no. 7, 074030 (2014) doi:10.1103/PhysRevD.90.074030 [arXiv:1408.5086 [hep-lat]].
- [17] O. Philipsen and C. Pinke, Phys. Rev. D **93**, no. 11, 114507 (2016) doi:10.1103/PhysRevD.93.114507 [arXiv:1602.06129 [hep-lat]].
- [18] F. Cuteri, O. Philipsen and A. Sciarra, arXiv:1711.05658 [hep-lat].
- [19] M. D'Elia, A. Di Giacomo and C. Pica, Phys. Rev. D **72**, 114510 (2005) doi:10.1103/PhysRevD.72.114510 [hep-lat/0503030].
- [20] G. Cossu, S. Aoki, H. Fukaya, S. Hashimoto, T. Kaneko, H. Matsufuru and J. I. Noaki, Phys. Rev. D **87**, no. 11, 114514 (2013) Erratum: [Phys. Rev. D **88**, no. 1, 019901 (2013)] doi:10.1103/PhysRevD.88.019901, 10.1103/PhysRevD.87.114514 [arXiv:1304.6145 [hep-lat]].
- [21] S. Aoki, H. Fukaya and Y. Taniguchi, Phys. Rev. D **86**, 114512 (2012) doi:10.1103/PhysRevD.86.114512 [arXiv:1209.2061 [hep-lat]].
- [22] M. Fukugita, H. Mino, M. Okawa and A. Ukawa, Phys. Rev. D **42**, 2936 (1990). doi:10.1103/PhysRevD.42.2936
- [23] C. W. Bernard, C. E. Detar, S. A. Gottlieb, U. M. Heller, J. Hetrick, K. Rummukainen, R. L. Sugar and D. Toussaint, Phys. Rev. D **61**, 054503 (2000) doi:10.1103/PhysRevD.61.054503 [hep-lat/9908008].
- [24] H. B. Meyer, PoS LATTICE **2015**, 014 (2016) [arXiv:1512.06634 [hep-lat]].
- [25] A. Bazavov *et al.* [HotQCD Collaboration], Phys. Rev. D **86**, 094503 (2012) doi:10.1103/PhysRevD.86.094503 [arXiv:1205.3535 [hep-lat]].
- [26] C. Bonati, P. de Forcrand, M. D'Elia, O. Philipsen and F. Sanfilippo, PoS LATTICE **2011**, 189 (2011) [arXiv:1201.2769 [hep-lat]].
- [27] A. Bazavov *et al.*, Phys. Rev. D **85**, 054503 (2012) doi:10.1103/PhysRevD.85.054503 [arXiv:1111.1710 [hep-lat]].
- [28] A. Bazavov *et al.* [MILC Collaboration], Rev. Mod. Phys. **82** 1349 (2010).
- [29] Z. Hao, G. M. von Hippel, R. R. Horgan, Q. J. Mason and H. D. Trotter, Phys. Rev. D **76**, 034507 (2007) doi:10.1103/PhysRevD.76.034507 [arXiv:0705.4660 [hep-lat]].
- [30] K. Symanzik, Nucl. Phys. B **226**, 187 (1983). doi:10.1016/0550-3213(83)90468-6
- [31] M. Luscher and P. Weisz, Phys. Lett. **158B**, 250 (1985). doi:10.1016/0370-2693(85)90966-9
- [32] G. P. Lepage and P. B. Mackenzie, Phys. Rev. D **48**, 2250 (1993) doi:10.1103/PhysRevD.48.2250 [hep-lat/9209022].
- [33] M. G. Alford, W. Dimm, G. P. Lepage, G. Hockney and P. B. Mackenzie, Phys. Lett. B **361**, 87 (1995) doi:10.1016/0370-2693(95)01131-9 [hep-lat/9507010].
- [34] A. Hart *et al.* [HPQCD Collaboration], Phys. Rev. D **79**, 074008 (2009) doi:10.1103/PhysRevD.79.074008 [arXiv:0812.0503 [hep-lat]].
- [35] E. Follana *et al.* [HPQCD and UKQCD Collaborations], Phys. Rev. D **75**, 054502 (2007) doi:10.1103/PhysRevD.75.054502 [hep-lat/0610092].
- [36] S. Naik, 1989 Nucl. Phys. B **316** 238 (1989).
- [37] C. W. Bernard *et al.* [MILC Collaboration], Phys. Rev. D **58** 014503 (1998).
- [38] P. Cea, L. Cosmai and A. Papa, Phys. Rev. D **89**, no. 7, 074512 (2014) doi:10.1103/PhysRevD.89.074512 [arXiv:1403.0821 [hep-lat]].
- [39] A. Bazavov *et al.* [MILC Collaboration], Phys. Rev. D **82**, 074501 (2010) doi:10.1103/PhysRevD.82.074501 [arXiv:1004.0342 [hep-lat]].
- [40] M. A. Clark and A. D. Kennedy, Nucl. Phys. Proc. Suppl. **129** 850 (2004).
- [41] M. A. Clark and A. D. Kennedy, Phys. Rev. D **75** 011502 (2007).
- [42] M. A. Clark and A. D. Kennedy, Phys. Rev. Lett. **98** 051601 (2007).
- [43] J.C. Sexton and D.H. Weingarten, Nucl. Phys. **B380**, 665 (1992).
- [44] T. Takaishi and P. De Forcrand, Phys. Rev. E **73** 036706 (2006).
- [45] I. P. Omeylan, I. M. Mryglod and R. Folk, Comp. Phys. Comm. **151** 272 (2003).
- [46] A. M. Ferrenberg and R. H. Swendsen, Phys. Rev. Lett. **63**, 1195 (1989).
- [47] A. Bazavov, H.-T. Ding, P. Hegde, F. Karsch, E. Laermann, S. Mukherjee, P. Petreczky and C. Schmidt, Phys. Rev. D **95**, no. 7, 074505 (2017) doi:10.1103/PhysRevD.95.074505 [arXiv:1701.03548 [hep-lat]].
- [48] S. T. Li and H. T. Ding, PoS LATTICE **2016**, 372 (2017) [arXiv:1702.01294 [hep-lat]].
- [49] P. de Forcrand, S. Kim and O. Philipsen, PoS LATTICE **2007**, 178 (2007) [arXiv:0711.0262 [hep-lat]].
- [50] G. Endrodi, Z. Fodor, S. D. Katz and K. K. Szabo, PoS LATTICE **2007**, 182 (2007) [arXiv:0710.0998 [hep-lat]].
- [51] <http://physics.utah.edu/~detar/milc/>.
- [52] <http://crd-legacy.lbl.gov/~dhbailey/mpdist/>.